Nonlinear Dyn (2024) 112:18665–18684
https://doi.org/10.1007/s11071-024-10040-z

RESEARCH

Pendulum-based hybrid system for multidirectional energy harvesting

Luã G. Costa · **Marcelo A. Savi**

Received: 10 April 2024 / Accepted: 17 July 2024 / Published online: 27 July 2024

Abstract This work presents a hybrid multidirectional mechanical energy harvester to enhance the performance of a cantilever-based harvester when subjected to multidirectional excitations. The multidirectional capabilities are achieved by employing a pendulum structure. Hybrid transduction is provided by combining a piezoelectric element and an electromagnetic transducer. A reduced-order model is presented based on the electromechanical Lagrangian formulation, and numerical analyses are performed to characterize the system behavior. A comparison based on energy harvesting performance is established among the novel multidirectional hybrid energy harvester (MHEH), the classical piezoelectric harvester (CPEH), and a multidirectional piezoelectric harvester (MPEH). Results show that the addition of the pendulum alone indeed provides multidirectional capabilities, but the overall performance can be reduced in some scenarios since it works as an energy absorber. This limitation is overcome by the hybridization strategy of the MHEH, by incorporating an electromagnetic transducer into the pendulum support. Overall, a significant improvement is achieved in all scenarios by utilizing the hybrid system.

L. G. Costa · M. A. Savi (✉)
COPPE - Mechanical Engineering Center for Nonlinear Mechanics, Universidade Federal do Rio de Janeiro, Rio de Janeiro, RJ 21941-914, Brazil
e-mail: savi@mecanica.coppe.ufrj.br

L. G. Costa
e-mail: guedes@mecanica.coppe.ufrj.br

Keywords Multidirectional energy harvesting · Hybrid energy harvesting · Smart materials · Nonlinear dynamics · Pendulum structures · Electromechanical systems

1 Introduction

Advancements throughout history have allowed human society to manipulate the environment and use the available Earth assets in their favor. The population growth together with the consumption of natural resources is leading the Earth complex system towards a critical planetary threshold that, if crossed, could irreversibly destabilize the dynamics that maintain the global ecological balance; this is often called the "point of no return" and underscores the urgency of sustainable resource management [43]. This context has encouraged the emergence of a growing number of initiatives, research endeavors, and development projects to explore renewable and sustainable alternatives to technological development, reflecting a collective recognition of the pressing need to shift away from the nowadays paradigms [27]. In this regard, the continuous evolution of semiconductor technology is enabling the reduction of power consumption in electronic systems [56]. This trend has sparked a growing interest in the potential of environmental mechanical energy sources, such as vibrations, sound, wind, and sea waves, as a viable alternative for charging small-to-medium-sized systems, including alternatives to tra-

ditional batteries. Mechanical energy sources offer an attractive solution to the challenge of sustainable energy, providing the possibility to power a wide range of devices, from small electronics to small urban centers [41,45].

Mechanical energy harvesting technology has a wide range of applications across diverse fields within self-powered wireless sensors, IoT (internet of things), and MEMs (micro-electro-mechanical systems) which have been the main focus of literature [18,28]. Nevertheless, large-scale systems also show a promising area of development [57]. Some examples of the potential applications of mechanical energy harvesting include capturing energy from traffic-induced vibrations [21,39], compressive loadings on pavements and buildings [20,46], and health monitoring of civil infrastructure [16]. In the biomedical field, it has the potential to harvest energy from the motion of organs such as the heart, lung, and diaphragm, to power active implantable medical devices such as pacemakers [13,17], and even monitor wildlife as shown by [31]. Additionally, numerous studies have investigated the powering of wearables through energy conversion from human motion [15,33,54]. Lastly, offshore deployments for wave energy harvesting [36] and health monitoring of vehicle components are also potential applications [30,44].

In order to harness the available ambient mechanical energy and effectively convert it into electrical energy, the transduction mechanisms are essential. Electromagnetic converters, triboelectric structures, and piezoelectric materials can be enumerated as some classical strategies to achieve this goal. Electromagnetic harvesters rely on the principle of electromagnetic induction, being commonly used in robust applications, ranging from micro to large scale applications [6]. In contrast, triboelectric structures use friction between two different materials to create an electric potential between two surfaces, making them more compact and suitable for nano to microscale applications [26]. On the other hand, piezoelectric materials are smart materials that convert mechanical into electrical energy through the reversible process of the piezoelectric effect, which produces a proportional charge as a result of the application of a mechanical field. Piezoelectric transducers can be applied to harvest energy from micro to large-scale applications [9].

The hybrid transduction combining different types of transducers is a trend to enhance system performance. This combination allows to exploitation of the unique advantages of each transducer, resulting in greater energy harvesting capacity. Depending on the transducer combinations, various applications can be realized. For instance, [8] utilized a Kresling origami structure that combined rotational triboelectric and piezoelectric/triboelectric nanoconverters in contact mode. This innovative approach allowed the structure to take advantage of the rotational movement, the generated strain and contact, resulting in a better energy harvesting performance. Similarly, [55] utilized both electromagnetic and triboelectric transducers to build a hybrid energy harvester based on rotation to scavenge biomechanical energy as a mobile power source. Egbe et al. [19] employed three different transduction mechanisms to enhance the conversion of wind energy to electrical energy through a rotational device to power sensors. Other researchers have also reported the use of various hybrid devices showing improved performance through the utilization of different conversion strategies [24,25,50,52]. By utilizing the unique advantages of each transducer, hybrid systems can indeed facilitate more efficient energy harvesting solutions.

The harvesters documented in the literature are resonators, including structural elements such as beams and plates. On this basis, their effectiveness in converting energy is limited to situations close to the resonant condition when operating in a linear regime. This limitation has motivated the use of nonlinear modulations, which can increase their operation bandwidth and enable better performance when subjected to environmental uncertainties. Multistable systems that are induced either by magnets or by post-buckled structures can be cited as one of the most common nonlinearity modulations found in the literature [10,14]. Compared to the linear systems, this class of harvester presents a better performance by increasing the maximum output power and operation bandwidth [42]. Non-smooth impact-driven modulations are also employed to enhance the operation bandwidth, but at the cost of the reduction of the maximum output power [3]. Besides, the mechanical wear caused by successive impacts can be a drawback of this kind of harvester. Adeodato et al. [2] and [53] showed that the synergistic use of smart materials can be a viable solution to control and tune the natural frequency of the harvester, increasing the operation bandwidth in different scenarios.

The design of different structures is also of concern trying to enhance energy harvesting capacity. In this regard, multimodal structures are proposed with multiple degrees of freedom. Caetano and Savi [4] proposed some structures with configurations optimized from circular plates to pizza-shaped with irregular slices. The multimodal pizza-shaped harvester presented a better performance than the classical beam harvester, increasing its broadband. Costa and Savi [12] proposed a compact multistable energy harvester composed of a dual beam nonlinear structure featuring two magnetic interactions and two piezoelectric transducers. The harvester presented a better performance than the conventional bistable harvester. In a subsequent work, it was revealed that this harvester can be configured to be monostable, bistable, or tetrastable. In general, it was shown that the tetrastability configuration has greater performance than its counterparts [11]. Rotational energy harvesters using piezoelectric, electrostatic, triboelectric, and electromagnetic transducers, with simple and complex structures are also reported in the literature [23].

Energy harvesting from multiple directions is another important aspect to be incorporated into the designs since energy sources have unavoidable uncertainties. It has been shown that the usage of pendulum structures to achieve multidirectionality is an interesting and effective solution [49]. Unlike classical cantilever-based piezoelectric energy harvesters, which primarily operate in a single direction, pendulum-based systems can harness energy from various directions. Pendulum structures have been used in mechanical energy harvesting systems, as demonstrated in recent studies [7,22,47]. Specifically, they can be used in some ways to incorporate multidirectional capabilities to the classical cantilever-based piezoelectric energy harvester, as demonstrated by [51], as well as [37,38] and [48]. Caetano and Savi [5] proposed a star-shaped harvester, comparing its performance with the counterpart version, without pendula. The proposed harvester presents a multimodal and multidirectional energy harvesting capacity. Other types of multidirectional mechanisms such as the complex 3-DoF frame structure proposed by [1], the tunable buckled piezoelectric film proposed by [34], and the rotational cam rotor-based energy harvester proposed by [29] are also reported.

Although pendulum structures are useful to confer multidirectional aspects to energy harvesters, a deep discussion about dynamical influence of the pendulum system is important since it can work as a dynamical absorber. Therefore, a comparison of these new cantilever-pendulum systems against the classical piezoelectric energy harvester needs to be performed accordingly, which is not addressed in the literature.

This work deals with an investigation of multidirectional mechanical energy harvesting, proposing an archetype reduced order model of a multidirectional hybrid pendulum-based energy harvester (MHEH). Specifically, MHEH is a modified version of the classical cantilever-based piezoelectric energy harvester. The pendulum-based system presents multidirectional coupling, allowing the conversion of the mechanical energy source directions that otherwise would be lost. A piezoelectric transducer is attached to a cantilever structure to convert energy from flexural oscillations, while an electromagnetic converter is attached to the pendulum to harness the rotational energy. Numerical simulations are performed in order to show that the addition of a pendulum structure into the cantilever-based energy harvester design is sufficient to provide efficient multidirectional capabilities. Results show that the usage of pendulum structures is advantageous if associated with an additional strategy to harness the rotational energy from the pendulum.

After this introduction, this work is organized as follows: Sect. 2 establishes the conceptual representation of three types of energy harvesters, representing the natural evolution of the classical piezoelectric energy harvester to the proposed multidirectional hybrid energy harvester. A theoretical model is developed to describe the qualitative characteristics of the three structures. Section 3 explores the advantages and disadvantages of using pendulum structures to achieve multidirectionality, and how to counteract them. Section 4 presents a numerical analysis to characterize the performance of the system by analyzing a set of important parameters such as the ratio between the natural frequencies of each direction, the electrical resistances, the electromechanical couplings, and the excitation characteristics. Finally, the conclusions are presented in Sect. 5.

2 Design and theoretical model

Consider the conceptual representation of three cantilever-based energy harvesters presented in Fig. 1. The first configuration is shown in Fig. 1a, representing the classical cantilever-based piezoelectric energy

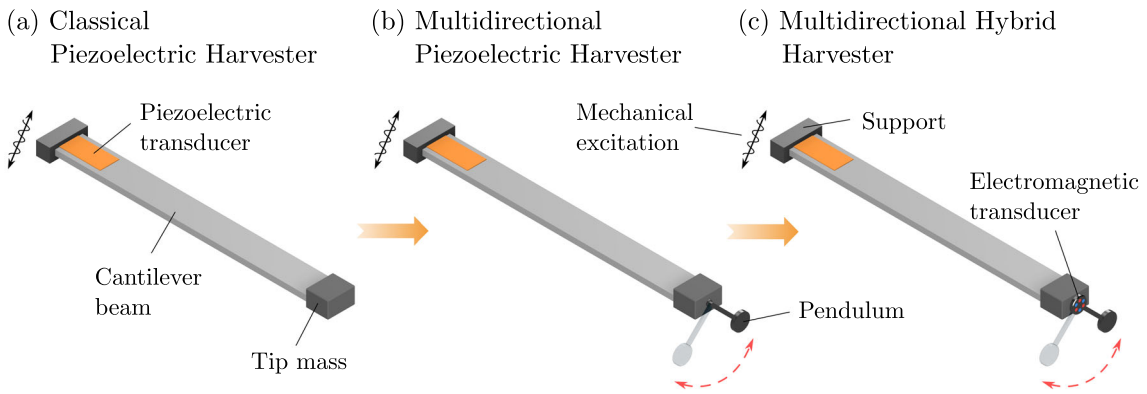

Fig. 1 Conceptual representation of the three types of energy harvesters. **a** The classical piezoelectric energy harvester (CPEH), composed of a piezoelectric transducer and a cantilever beam structure with a tip mass. **b** the multidirectional piezoelectric energy harvester (MPEH), composed by the CPEH plus the addition of a pendulum structure. **c** The proposed multidirectional hybrid energy harvester (MHEH) composed of the MPEH plus the addition of an electromagnetic transducer at the pendulum support

harvester (CPEH), composed by a piezoelectric transducer attached to a structural beam element, a support where the beam is embedded, and a tip mass at its free end. The second design, displayed in Fig. 1b, shows the multidirectional piezoelectric harvester (MPEH) incorporating the pendulum in the classical design. This layout leverages the planar motion of the pendulum to transmit the input energy from one Cartesian direction to another. Finally, Fig. 1c shows the proposed multidirectional hybrid energy harvester (MHEH), which incorporates an additional electromagnetic transducer at the support of the pendulum in order to harness its rotational energy.

The proposed novel design incorporates a pendulum harvester to the classical cantilever-based energy harvester in order to achieve efficient multidirectional capabilities. In the next subsection, an archetype model is developed containing the key dynamical characteristics of each one of the three configurations of Fig. 1. This model allows one to develop a numerical investigation to establish the advantages of using pendulum structures to achieve multidirectional capabilities in the classical cantilever-based energy harvesters.

2.1 Physical modeling

The energy harvesters presented in Fig. 1 can be represented by the general archetype model depicted in Fig. 2. The model considers the beam main structure with effective mass m_s, and a pendulum-type element of effective mass m_p attached to it. The equivalent stiffness and damping coefficients are represented by k_i $(i = x, z, pz)$ and c_j $(j = x, z, em, p)$, in which subscripts are related to the direction or an element within the system. Subscript x and z refer to the plane directions, while subscript p refers to the pendulum; subscripts pz and em refer to the piezoelectric and electromagnetic transducers, respectively. Two transducers are attached to the system: a piezoelectric element with an electromechanical coupling term, θ_{pz} and an equivalent stiffness, k_{pz}, in the z direction of the structure; and an electromagnetic energy converter attached to the support of the pendulum with an electromagnetic coupling term, θ_{em}, and a magnetic damping coefficient c_{em}. The transducers are represented by an equivalent circuit. The piezoelectric element can be represented by a circuit depicted in Fig. 2b, with an internal capacitance, C_{pz}, connected in parallel to internal resistance, R_{ipz}, and an induced current related to the electromechanical coupling, $I_{pz}(t) = \theta_{pz}\dot{z}(t)$. An external load resistance, R_{lpz}, is also attached to the piezoelectric element. Additionally, the electromagnetic transducer is represented by the circuit depicted in Fig. 2c, with a voltage source, $v_{em}(t) = \theta_{em}\dot{\phi}(t)$, connected in series with an equivalent internal inductance, L_{em}, an internal resistance R_{iem}, and external load resistance, R_{lem}. The equivalent resistance of the piezoelectric circuit is represented by $R_{pz} = R_{ipz}R_{lpz}/\left(R_{lpz} + R_{ipz}\right)$, while

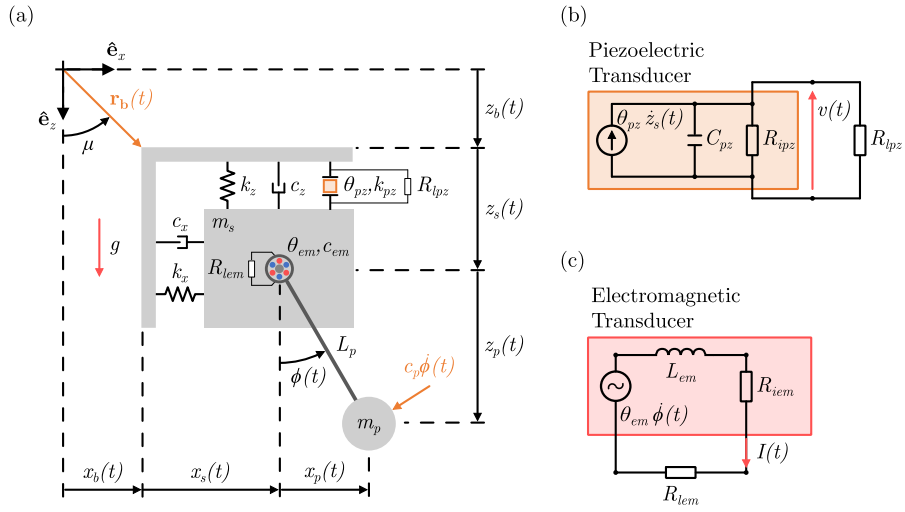

Fig. 2 **a** Archetype representing the Hybrid Multidirectional Energy Harvester. **b** The equivalent circuit of the piezoelectric transducer attached to a resistance. **c** The equivalent circuit of the electromagnetic transducer attached to a resistance

the equivalent resistance of the electromagnetic circuit is represented by $R_{em} = R_{iem} + R_{lem}$.

The effects of gravity, g, are considered, and the system is subjected to a multidirectional excitation represented by the vector $\mathbf{r_b}(t) = r_b(t)\left[\sin(\mu)\hat{\mathbf{e}}_x + \cos(\mu)\hat{\mathbf{e}}_z\right]$, where the bold notation refers to vectors and italic notation refers to scalars; μ is the angle between the external excitation vector $\mathbf{r_b}(t)$ and the z direction, and $r_b(t)$ is the excitation function; the vectors $\hat{\mathbf{e}}_x$ and $\hat{\mathbf{e}}_z$ are the base vectors of each Cartesian direction, x and z, respectively.

The absolute structure position can be written as follows,

$$\begin{aligned}\mathbf{r}_s(t) &= [x_b(t) + x_s(t)]\,\hat{\mathbf{e}}_x + [z_b(t) + z_s(t)]\,\hat{\mathbf{e}}_z \\ &= [x_b(t) + x(t)]\,\hat{\mathbf{e}}_x + [z_b(t) + z(t) + z_{st}]\,\hat{\mathbf{e}}_z,\end{aligned} \tag{1}$$

where $x(t)$ and $z(t)$ are the relative positions in which the system oscillates with respect to the equilibrium position, and $z_{st} = (m_s + m_p)\,g/(k_z + k_{pz})$ is the static deflection of the structure due to gravity action. Also, the absolute position of the pendulum is given by

$$\begin{aligned}\mathbf{r}_p(t) &= \left[x_b(t) + x(t) + x_p(t)\right]\hat{\mathbf{e}}_x \\ &\quad + \left[z_b(t) + z(t) + z_{st} + z_p(t)\right]\hat{\mathbf{e}}_z \\ &= \left[x_b(t) + x(t) + L_p\sin(\phi(t))\right]\hat{\mathbf{e}}_x + [z_b(t) \\ &\quad + z(t) + z_{st} + L_p\cos(\phi(t))\right]\hat{\mathbf{e}}_z.\end{aligned} \tag{2}$$

By considering an energetic approach, the total kinetic energy can be written as the composition of the structure and the pendulum kinetic energies as follows,

$$\begin{aligned}T &= T_s + T_p \\ &= \frac{1}{2}m_s\dot{\mathbf{r}}_s(t)\cdot\dot{\mathbf{r}}_s(t) + \frac{1}{2}m_p\dot{\mathbf{r}}_p(t)\cdot\dot{\mathbf{r}}_p(t) \\ &= \frac{1}{2}m_p\left\{\left[\dot{x}(t) + \dot{x}_b(t) + L_p\dot{\phi}(t)\cos(\phi(t))\right]^2\right. \\ &\quad \left. + \left[\dot{z}(t) + \dot{z}_b(t) - L_p\dot{\phi}(t)\sin(\phi(t))\right]^2\right\} \\ &\quad + \frac{1}{2}m_s\left\{[\dot{x}(t) + \dot{x}_b(t)]^2 + [\dot{z}(t) + \dot{z}_b(t)]^2\right\}.\end{aligned} \tag{3}$$

The structure and piezoelectric element constitutive behaviors are assumed to be linear and, therefore, the total restitution forces of the structure and the piezoelectric elements are defined by

$$f_x(t) = -k_x x(t), \tag{4}$$

$$f_z(t) = -k_z z(t), \tag{5}$$

$$f_{pz}(t) = -k_{pz} z(t), \tag{6}$$

resulting in the total potential energy, written as the sum of the main structure, piezoelectric element, and pendulum potential energies,

$$\begin{aligned}U &= U_s + U_p \\ &= -\int_0^{x_s(t)} f_x(t)\,dx - \int_0^{z_s(t)}\left[f_z(t) + f_{pz}(t)\right]dz \\ &\quad - \int_0^{z_b(t)+z_s(t)} m_s g\,dz - \int_0^{z_b(t)+z_s(t)+z_p(t)} m_p g\,dz \\ &= \frac{1}{2}k_x x(t)^2 + \frac{1}{2}(k_z + k_{pz})\,[z(t) + z_{st}]^2 \\ &\quad - m_s g\,[z_b(t) + z(t) + z_{st}] \\ &\quad - m_p g\left[z_b(t) + z(t) + z_{st} + L_p\cos(\phi(t))\right].\end{aligned} \tag{7}$$

The electromechanical coupling of the piezoelectric transducer, θ_{pz}, is related to the induced current, $I_{pz}(t)$, being determined by the properties of the piezoelectric material, its geometry and dimensions. In contrast, the electromechanical coupling of the electromagnetic transducer, θ_{em}, is related to the induced voltage, $v_{em}(t)$, being determined by the geometric characteristics of the coil(s), the properties of the magnet(s) within the converter, the intensity of its magnetic field(s), and the position and distribution of the elements within the transducer. Often, it is possible to determine these two quantities analytically, nevertheless, either finite element analysis or experimental methods are required for complex structures. Another possibility is that these coupling mechanisms can dynamically change depending on the state of the system. For the sake of simplicity, this work considers constant coupling coefficients.

From this perspective, consider the linear relation between the flux linkage, $\psi(t)$, and the voltage, $v(t)$, across the piezoelectric circuit as $\dot{\psi}(t) = v(t)$, and the linear relation between the charge, $q(t)$, and the current, $I(t)$, flowing in the electromagnetic circuit as $\dot{q}(t) = I(t)$. The total electrical domain energy can be represented by the sum of the total electric energy of the piezoelectric element, W_e and the total magnetic energy of the electromagnetic transducer, W_m: $W = W_e + W_m$.

The total energy of the piezoelectric transducer, W_e, is composed by the sum of the electric energy in the capacitance, W_C, and the piezoelectric energy, W_{pz}, being expressed as follows,

$$W_e = W_C + W_{pz} = \frac{1}{2} C_{pz} \dot{\psi}(t)^2 + \theta_{pz} \dot{\psi}(t) z(t). \quad (8)$$

On the other hand, the total energy of the electromagnetic transducer, W_m, is composed by the sum of the magnetic energy in the inductance, W_L, and the electromagnetic coupling energy, W_{em}.

$$W_m = W_L + W_{em} = \frac{1}{2} L_{em} \dot{q}(t)^2 + \theta_{em} \dot{q}(t) \phi(t). \quad (9)$$

Details of this formulation can be seen in [40].

The system dissipation can be modeled using dissipation functions as discussed in [35] and [40]. Three major sources are identified: the mechanical dissipation function acting on the main structure, D_s; the dissipation function acting on the pendulum, D_ϕ; and the electrical dissipation in the circuits due to resistance elements, D_R. Thus, the total dissipation can be written as $D = D_s + D_\phi + D_R$.

The main structure dissipation is mainly composed of the viscous sources, split into D_x, associated with x-direction and D_z, related to z direction,

$$D_s = D_x + D_z = \frac{1}{2} c_x \dot{x}(t)^2 + \frac{1}{2} c_z \dot{z}(t)^2, \quad (10)$$

The pendulum dissipation is mainly composed of pendulum viscous dissipation, D_{ϕ_e}, and internal magnetic dissipation within the magnetic transducer, D_{ϕ_i}. Therefore, it is written [32],

$$D_\phi = D_{\phi_e} + D_{\phi_i} = \frac{1}{2} c_p L_p \dot{\phi}(t)^2 + \frac{1}{2} c_{em} \dot{\phi}(t)^2, \quad (11)$$

Finally, the dissipation acting on the electrical domain is associated with the resistive elements represented by D_{pz}, associated with piezoelectric circuit, and D_{em}, related to electromagnetic circuits. Therefore, the following expression is achieved,

$$D_R = D_{pz} + D_{em} = \frac{1}{2} \frac{\dot{\psi}(t)^2}{R_{pz}} + \frac{1}{2} R_{em} \dot{q}(t)^2, \quad (12)$$

On this basis, the Lagrangian can be defined as $\mathcal{L} = T - U + W$, where the electromechanical system is associated with five generalized coordinates (three mechanical and two electrical), $\mathbf{Q} = [x(t), z(t), \phi(t), \psi(t), q(t)]$. Therefore, by applying the Euler-Lagrange method, the following equation is achieved,

$$\frac{d}{dt}\left(\frac{\partial \mathcal{L}}{\partial \dot{Q}_i}\right) - \frac{\partial \mathcal{L}}{\partial Q_i} + \frac{\partial D}{\partial \dot{Q}_i} = 0. \quad (13)$$

Suppressing the (t) in the notation of the generalized coordinates, the electromechanical equations of motion can be written as a system of equations related to the state variables x, z, ϕ, v and I:

$$\begin{aligned} &\left(m_s + m_p\right)\ddot{x} + c_x \dot{x} + k_x x \\ &\quad + m_p L_p \left[\ddot{\phi}\cos(\phi) - \dot{\phi}^2 \sin(\phi)\right] \\ &\quad = -\left(m_s + m_p\right)\ddot{x}_b; \end{aligned} \quad (14)$$

$$\begin{aligned}&\left(m_s+m_p\right)\ddot{z}+c_z\dot{z}+\left(k_z+k_{pzt}\right)z-\theta_{pz}v\\&\quad-m_pL_p\left[\ddot{\phi}\sin\left(\phi\right)+\dot{\phi}^2\cos\left(\phi\right)\right]\\&=-\left(m_s+m_p\right)\ddot{z}_b;\end{aligned}\tag{15}$$

$$\begin{aligned}&m_pL_p^2\ddot{\phi}+(c_{em}+c_pL_p)\dot{\phi}\\&\quad+m_pL_p\left[\ddot{x}\cos\left(\phi\right)+(g-\ddot{z})\sin\left(\phi\right)\right]\\&\quad-\theta_{em}I=\\&m_pL_p\left[\ddot{z}_b\sin\left(\phi\right)-\ddot{x}_b\cos\left(\phi\right)\right];\end{aligned}\tag{16}$$

$$C_{pz}\dot{v}+\frac{v}{R_{pz}}+\theta_{pz}\dot{z}=0;\tag{17}$$

$$L_{em}\dot{I}+R_{em}I+\theta_{em}\dot{\phi}=0.\tag{18}$$

By assuming a harmonic external stimulus:

$$\mathbf{r_b}=x_b\hat{\mathbf{e}}_x+z_b\hat{\mathbf{e}}_z=A\sin\left(\omega t\right)\left[\sin\left(\mu\right)\hat{\mathbf{e}}_x+\cos\left(\mu\right)\hat{\mathbf{e}}_z\right].\tag{19}$$

Thus,

$$\begin{aligned}\ddot{\mathbf{r}}_\mathbf{b}&=\ddot{x}_b\hat{\mathbf{e}}_x+\ddot{z}_b\hat{\mathbf{e}}_z\\&=-A\omega^2\sin\left(\omega t\right)\left[\sin\left(\mu\right)\hat{\mathbf{e}}_x+\cos\left(\mu\right)\hat{\mathbf{e}}_z\right].\end{aligned}\tag{20}$$

Here A is the amplitude and ω is the frequency of excitation.

In order to generalize the analysis, a normalization approach is performed by considering a reference length, L, a reference voltage V, and a reference current $\mathcal{I}$, resulting in the following dimensionless electromechanical equations:

$$\begin{aligned}&(1+\rho)\,\ddot{\bar{x}}+2\zeta_x\dot{\bar{x}}+\Omega_s^2\bar{x}+\rho\ell\left[\ddot{\bar{\phi}}\cos\left(\bar{\phi}\right)-\dot{\bar{\phi}}^2\sin\left(\bar{\phi}\right)\right]\\&\quad=-(1+\rho)\ddot{\bar{x}}_b;\end{aligned}\tag{21}$$

$$\begin{aligned}&(1+\rho)\,\ddot{\bar{z}}+2\zeta_z\dot{\bar{z}}+\bar{z}-\chi_{pz}\bar{v}\\&\quad-\rho\ell\left[\ddot{\bar{\phi}}\sin\left(\bar{\phi}\right)+\dot{\bar{\phi}}^2\cos\left(\bar{\phi}\right)\right]\\&\quad=-(1+\rho)\ddot{\bar{z}}_b;\end{aligned}\tag{22}$$

$$\begin{aligned}&\ddot{\bar{\phi}}+2\zeta_\phi\dot{\bar{\phi}}+\Omega_\phi^2\sin\left(\bar{\phi}\right)-\chi_{em}\bar{I}\\&\quad+\frac{1}{\ell}\left[\ddot{\bar{x}}\cos\left(\bar{\phi}\right)-\ddot{\bar{z}}\sin\left(\bar{\phi}\right)\right]\\&\quad=\frac{1}{\ell}\left[\ddot{\bar{z}}_b\sin\left(\bar{\phi}\right)-\ddot{\bar{x}}_b\cos\left(\bar{\phi}\right)\right];\end{aligned}\tag{23}$$

$$\dot{\bar{v}}+\frac{\bar{v}}{\varphi_{pz}}+\kappa_{pz}\dot{\bar{z}}=0;\tag{24}$$

$$\dot{\bar{I}}+\varphi_{em}\bar{I}+\kappa_{em}\dot{\bar{\phi}}=0.\tag{25}$$

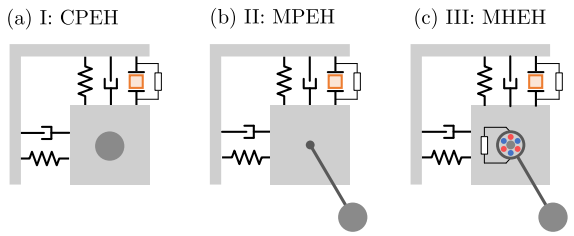

Fig. 3 Equivalent models of **a** Case I: The classical linear piezoelectric energy harvester (CPEH). **b** Case II: The multidirectional piezoelectric energy harvester (MPEH), with the multidirectionality induced by the pendulum structure attached to the mass. **c** Case III: The multidirectional hybrid energy harvester (MHEH), proposed in this work. The hybridization is achieved by the simultaneous usage of a piezoelectric and an electromagnetic transducer

These equations are related to the dimensionless parameters presented in Table 1 together with typical values.

This model allows the representation of all three harvesters depicted in Fig. 1, enabling further comparison among them. The modeling of the CPEH is achieved by maintaining the pendulum mass, reducing the pendulum length to zero, and removing the electromagnetic transducer as illustrated in Fig. 3a, denoted as Case I. This is equivalent of making the parameters $\zeta_\phi = \Omega_\phi = \ell = \chi_{em} = \kappa_{em} = \varphi_{em} = 0$. Case II, depicted in Fig. 3b, represents the model for the MPEH. This configuration can be achieved by removing the electromagnetic transducer, making $\chi_{em} = \kappa_{em} = \varphi_{em} = 0$. Finally, Case III refers to the proposed MHEH, with the pendulum structure and the electromagnetic converter, being represented in Fig. 3c.

2.2 Performance metrics

The performance of the energy harvesting system is evaluated with the definition of the electrical power associated with both piezoelectric and electromagnetic circuits. The total instantaneous electrical power consists of the sum of the instantaneous electrical power in each circuit, as represented by Eq. 26. Thus, the average electrical power, defined over the interval $t_0 \leq t \leq t_f$, is represented by Eq. 27, where v^{RMS} and I^{RMS} are the root-mean-square (RMS) of the output voltage of the piezoelectric circuit and the output current of the electromagnetic circuit, respectively, and is defined as depicted in Eq. 28.

Table 1 System parameters and values used in the analyses

Parameter description	Symbol	Definition	Value
Natural frequency of the main structure in x	ω_x	$\sqrt{k_x/m_s}$	–
Natural frequency of the main structure in z	ω_z	$\sqrt{k_z/m_s}$	–
Linearized natural frequency of the pendulum	ω_ϕ	$\sqrt{g/L_p}$	–
Normalized time	τ	$\omega_z t$	–
Normalized x displacement of the main structure	$\bar{x}(\tau)$	$x(t)/L$	–
Normalized z displacement of the main structure	$\bar{z}(\tau)$	$z(t)/L$	–
Normalized angle of the pendulum structure	$\bar{\phi}(\tau)$	$\phi(t)$	–
Normalized voltage of the piezoelectric circuit	$\bar{v}(\tau)$	$v(t)/V$	–
Normalized current of the electromagnetic circuit	$\bar{I}(\tau)$	$I(t)/\mathcal{I}$	–
Normalized base excitation frequency	Ω	ω/ω_z	$0.01 \rightarrow 2$
Normalized base excitation amplitude	γ	A/L	0.1, 0.25, 0.5
Normalized angle of the base excitation vector $\mathbf{r_b}(t)$	$\bar{\mu}$	μ	0°, 45°, 90°
Normalized base excitation displacement in the x direction	$\bar{x}_b(\tau)$	$\gamma \sin(\Omega\tau)\sin(\bar{\mu})$	–
Normalized base excitation displacement in the z direction	$\bar{z}_b(\tau)$	$\gamma \sin(\Omega\tau)\cos(\bar{\mu})$	–
Ratio of masses	ρ	m_p/m_s	0.5
Normalized damping coefficient of the main structure in x	ζ_x	$c_x/(2\omega_z m_s)$	0.025
Normalized damping coefficient of the main structure in z	ζ_z	$c_z/(2\omega_z m_s)$	0.025
Normalized total damping coefficient of the pendulum structure	ζ_ϕ	$\frac{[(c_{em}/L_p)+c_p]}{2\omega_z L_p m_s}$	0.0025
Ratio of natural frequencies of the main structure	Ω_s	ω_x/ω_z	0.5, 1, 1.5
Ratio of natural frequencies of the pendulum and the z direction	Ω_ϕ	ω_ϕ/ω_z	0.05
Normalized pendulum length	ℓ	L_p/L	1
Normalized piezoelectric coupling in the mechanical ODE	χ_{pz}	$\theta_{pz}V/(k_z L)$	0.05
Normalized electromagnetic coupling in the mechanical ODE	χ_{em}	$\theta_{em}\mathcal{I}/(\rho k_z L_p^2)$	$\eta\chi_{pz}$
Normalized piezoelectric coupling in the piezo circuit ODE	κ_{pz}	$\theta_{pz}L/(C_{pz}V)$	0.5
Normalized EM coupling in the electromagnetic circuit ODE	κ_{em}	$\theta_{em}/(L_{em}\mathcal{I})$	$\eta\kappa_{pz}$
Normalized equivalent resistance of the piezoelectric circuit	φ_{pz}	$C_{pz}R_{pz}\omega_z$	$0.2 \rightarrow 100$
Normalized equivalent resistance of the electromagnetic circuit	φ_{em}	$R_{em}/(L_{em}\omega_z)$	$0.01 \rightarrow 5$
Ratio between electromechanical couplings	η	$\chi_{em}/\chi_{pz} = \kappa_{em}/\kappa_{pz}$	$0.2 \rightarrow 1.0$
Normalized electrical output power of the piezoelectric circuit	$\bar{P}_{pz}(\tau)$	$P_{pz}(t)/(C_{pz}\omega_z V^2)$	–
Normalized electrical output power of the electromagnetic circuit	$\bar{P}_{em}(\tau)$	$P_{em}(t)/(L_{em}\omega_z\mathcal{I}^2)$	–

$$P = P_{pz} + P_{em} = \frac{1}{R_{pz}}v^2 + R_{em}I^2, \tag{26}$$

$$P_{\text{avg}} = \frac{1}{t_f - t_0}\int_{t_0}^{t_f} P\,dt = \frac{1}{R_{pz}}\left(v^{\text{RMS}}\right)^2 + R_{em}\left(I^{\text{RMS}}\right)^2, \tag{27}$$

where the RMS of any quantity can be defined as:

$$\square^{\text{RMS}} = \sqrt{\frac{1}{t_f - t_0}\int_{t_0}^{t_f}[\square(t)]^2\,dt}. \tag{28}$$

Furthermore, based on these concepts and according to Table 1, the normalized average electrical output power can be determined as described in Eq. 29.

$$\bar{P}_{\text{avg}} = \bar{P}_{pz} + \bar{P}_{\text{em}} = \frac{1}{\varphi_{pz}}\left(\bar{v}^{\text{RMS}}\right)^2 + \varphi_{em}\left(\bar{I}^{\text{RMS}}\right)^2. \tag{29}$$

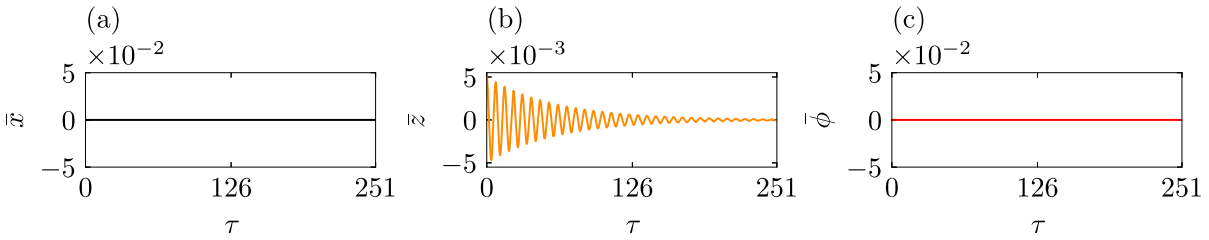

Fig. 4 Time series of the free response of the system as the structure is released from an arbitrary $\bar{z}$ initial position: **a** mass' relative horizontal position, $\bar{x}$; **b** mass' relative vertical position, $\bar{z}$; and **c** pendulum angular position, $\bar{\phi}$. The piezoelectric and electromagnetic transducers are excluded from the analysis, that is, $\chi_{pz} = \kappa_{pz} = \varphi_{pz} = \chi_{em} = \kappa_{em} = \varphi_{em} = 0$

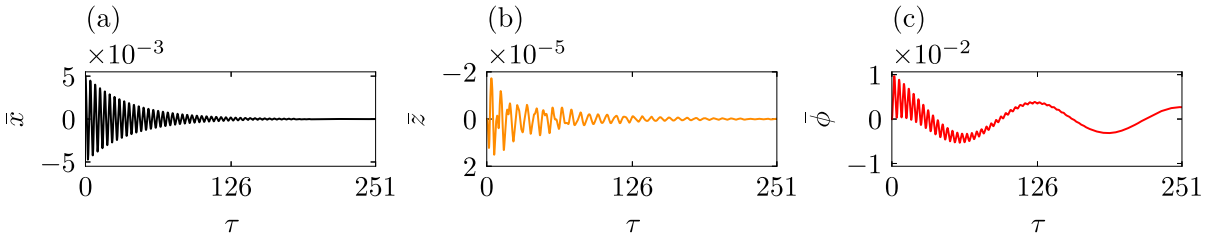

Fig. 5 Time series of the free response of the system as the structure is released from an arbitrary $\bar{x}$ initial position: **a** mass' relative horizontal position, $\bar{x}$; **b** mass' relative vertical position, $\bar{z}$; and **c** pendulum angular position, $\bar{\phi}$. The piezoelectric and electromagnetic transducers are excluded from the analysis, that is, $\chi_{pz} = \kappa_{pz} = \varphi_{pz} = \chi_{em} = \kappa_{em} = \varphi_{em} = 0$

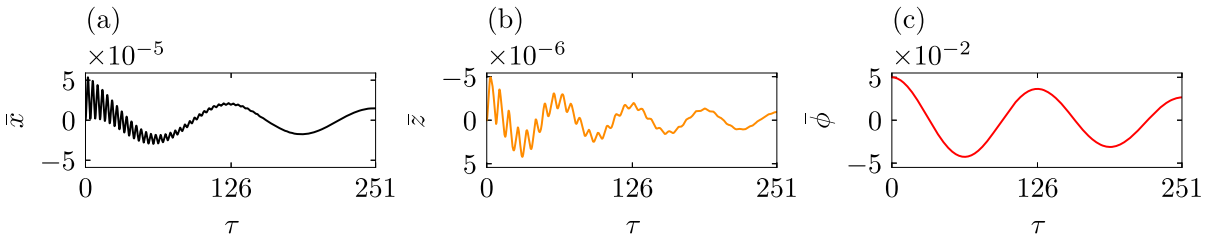

Fig. 6 Time series of the free response of the system as the pendulum is released from an arbitrary $\bar{\phi}$ initial angle: **a** mass' relative horizontal position, $\bar{x}$; **b** mass' relative vertical position, $\bar{z}$; and **c** pendulum angular position, $\bar{\phi}$. The piezoelectric and electromagnetic transducers are excluded from the analysis, that is, $\chi_{pz} = \kappa_{pz} = \varphi_{pz} = \chi_{em} = \kappa_{em} = \varphi_{em} = 0$

3 Multidirectional energy harvesting

This section evaluates the main characteristics of the energy harvester showing that the pendulum structure can be used to achieve multidirectionality in mechanical structures due to its capability to diffuse energy between different directions within the system. Numerical simulations carried out employing the fourth order Runge–Kutta scheme, considering a time step $\Delta\tau = 2\pi/(N\Omega)$, with $N = 6000$, defined after a convergence analysis. Dynamical observations are treated together with performance.

In order to illustrate the multidirectionality concept, consider the free responses of the system ($\gamma = \Omega = \bar{\mu} = 0$) with the following structural parameters: $\Omega_s = 1.5$ and $\Omega_\phi = 0.05$. Besides, the piezoelectric and electromagnetic transducers are excluded from the analysis, setting $\chi_{pz} = \kappa_{pz} = \varphi_{pz} = \chi_{em} = \kappa_{em} = \varphi_{em} = 0$. The remaining parameters are listed in Table 1. The idea is to show that energy can flow among the mechanical coordinates, which is shown in Figs. 4, 5 and 6 that present free responses imposed by different perturbations and represented by $\bar{x}$, $\bar{z}$ and $\bar{\phi}$.

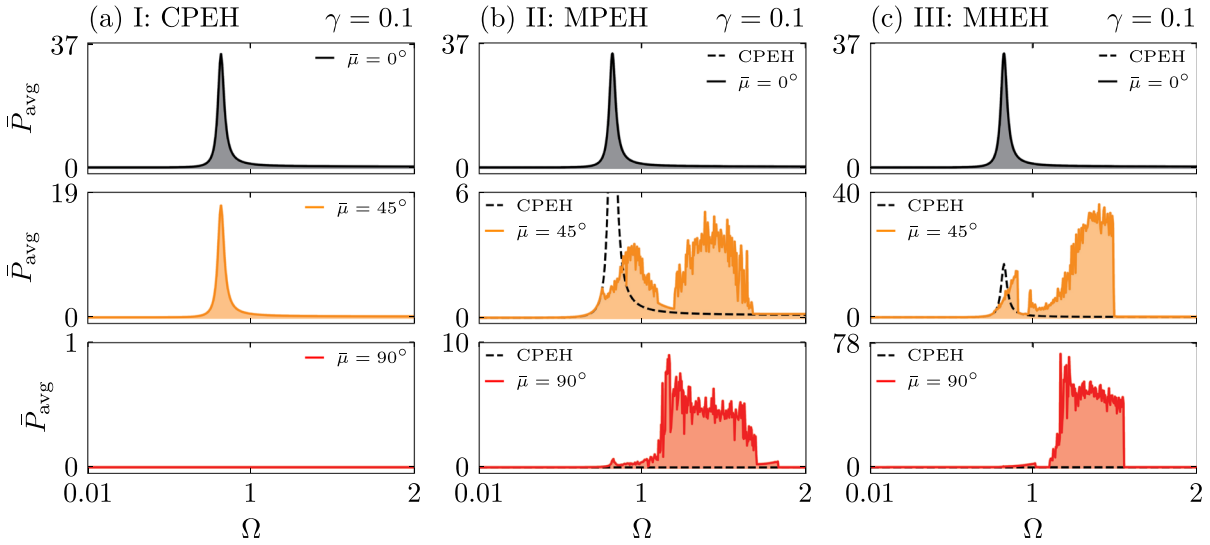

Fig. 7 $\bar{P}_{avg} \times \Omega$ diagrams for the Cases I, II, and III represented in Fig. 3 excited with different angles $\bar{\mu}$ for a normalized excitation amplitude of $\gamma = 0.1$. **a** Classical linear piezoelectric energy harvester (CPEH). **b** A comparison between the CPEH (dashed black lines) and the multidirectional piezoelectric energy harvester (MPEH). **c** A comparison between the CPEH (dashed black lines) and the proposed multidirectional hybrid energy harvester (MHEH). The values of $\bar{P}_{avg}$ are scaled by $\times 10^3$

Figure 4 shows a scenario in which the structure is perturbed with an arbitrary initial position in the $\bar{z}$ direction, while the pendulum $\bar{\phi}$ and the position of the structure $\bar{x}$ direction remain stationary at their initial condition. As time progresses, it is observed that the structure oscillates in the $\bar{z}$ direction, while the pendulum and the structure remain stationary at rest. This behavior is expected since the system is ideal and unperturbed in the other directions. In contrast, when the $\bar{x}$ direction is perturbed, energy is transmitted from the $\bar{x}$ direction to the pendulum, and from the pendulum to the $\bar{z}$ direction. This scenario is depicted in Fig. 5. Furthermore, Fig. 6 shows that when the pendulum is released from an arbitrary $\bar{\phi}$ initial angle, the energy is simultaneously transferred from the pendulum to both $\bar{x}$ and $\bar{z}$ directions. This analysis highlights the pendulum as an energy bridge between directions.

Energy harvesting assessment is now in focus, comparing the three energy harvesters illustrated in Fig. 1. For that, consider their equivalent models as established in Fig. 3. The electromagnetic transducer parameters utilized are of the following: $\chi_{em} = 0.04$, $\varphi_{em} = 0.25$, $\kappa_{em} = 0.4$. The remaining non-zero parameters are utilized as presented in Table 1.

The performance of each system is assessed across a range of frequencies by imposing three different excitation angles for each case, defining different multidirectional energy sources: $\bar{\mu} = 0°$, a unidirectional case; $\bar{\mu} = 45°$, a multidirectional case; and $\bar{\mu} = 90°$, an opposite case of the unidirectional source. Diagrams $\bar{P}_{avg} \times \Omega$ presented in Figs. 7, 8 and 9, are built using $\bar{x}_0 = \dot{\bar{x}}_0 = \bar{z}_0 = \dot{\bar{z}}_0 = \bar{\phi}_0 = \dot{\bar{\phi}}_0 = \bar{v}_0 = \bar{I}_0 = 0$ as initial conditions. An up-sweep test with 500 steps of the normalized frequency, Ω, is performed. For each step, $\Delta\Omega$, 800 excitation periods, T, are imposed at each integration, with the last 150 considered to be steady state. The value of the steady state average output power, $\bar{P}_{avg}$, is computed for each step. As Ω increases, the dynamics of the system are maintained, that is, besides for the first value of Ω, the initial conditions of each point in the diagram correspond to the end state of the preceding point. Different excitation levels of $\gamma = 0.1$, $\gamma = 0.25$, and $\gamma = 0.5$ are considered.

In each Figure, the first column (a) illustrates the performance of Case I: CPEH. It is observed that when the excitation angle, $\bar{\mu}$, is set to 0°, the system achieves maximum performance as the direction of excitation aligns parallel to the $\hat{\mathbf{e}}_z$ axis. However, as the angle $\bar{\mu}$ increases, the maximum output power diminishes gradually until it reaches zero at $\bar{\mu} = 90°$ when the excitation becomes perpendicular to the $\hat{\mathbf{e}}_z$ axis. Consequently, for excitation angles other than $\bar{\mu} = 0°$ and

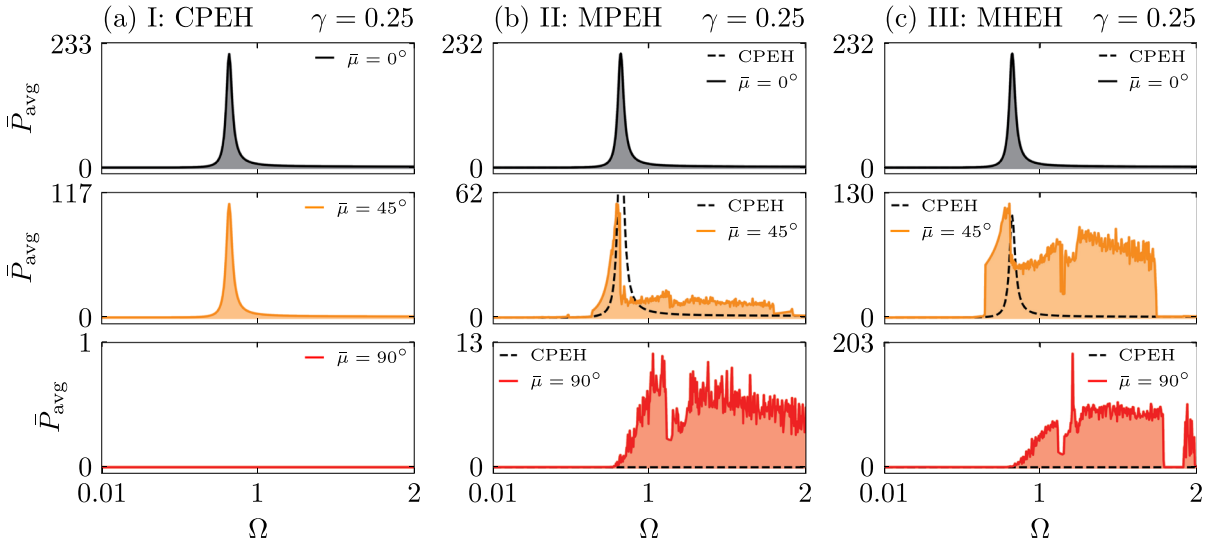

Fig. 8 $\bar{P}_{\text{avg}} \times \Omega$ diagrams for the Cases I, II, and III represented in Fig. 3 excited with different angles $\bar{\mu}$ for a normalized excitation amplitude of $\gamma = 0.25$. **a** Classical linear piezoelectric energy harvester (CPEH). **b** A comparison between the CPEH (dashed black lines) and the multidirectional piezoelectric energy harvester (MPEH). **c** A comparison between the CPEH (dashed black lines) and the proposed multidirectional hybrid energy harvester (MHEH). The values of $\bar{P}_{\text{avg}}$ are scaled by $\times 10^3$

$\bar{\mu} = 180°$, the CPEH system experiences a loss of valuable energy from the environment.

This issue is addressed by incorporating a pendulum structure that achieves multidirectionality (referred to as Case II: MPEH) as demonstrated by [51], as well as [37,38]. Figures 7b, 8b and 9b display the performance for this kind of harvester. For an excitation angle of $\bar{\mu} = 0°$, the performance of the MPEH is identical to that of the CPEH as there is no resulting motion from the pendulum. In contrast, for an excitation angle of $\bar{\mu} = 90°$ the advantages of utilizing a pendulum structure to facilitate energy transfer between directions become evident. In this scenario, the system is capable of effectively harvesting energy from all directions. However, for intermediate angles between $0° < \bar{\mu} < 90°$ it exhibits a drawback, demonstrating lower performance (lower maximum output power) compared to the CPEH in certain scenarios. This is due to the pendulum acting as an energy absorber.

In order to deal with this matter, an electromagnetic transducer has been integrated into the system to harness the rotational energy, enabling a portion of the mechanical energy absorbed by the pendulum to be converted into electrical energy. On this basis, a hybrid system is of concern, represented by Case III: MHEH. The performance of this harvester is presented in Figs. 7c, 8c and 9c. Similar to the previous case, for an angle of $\bar{\mu} = 0°$, the performance of the MHEH is equivalent to the CPEH as there is no resulting motion of the pendulum. However, for angles of $\bar{\mu} = 45°$ and $\bar{\mu} = 90°$, there is an impressive increase of performance in both maximum output power and bandwidth when compared to the CPEH.

These results clearly show that the MHEH (Multidirectional Hybrid Energy Harvester) not only retains the desirable characteristics of the MPEH (Multidirectional Piezoelectric Energy Harvester) but can also effectively address its limitations. This highlights the importance of incorporating the additional strategy to harness the rotational energy when utilizing pendulum structures for efficient multidirectional piezoelectric energy harvesting applications.

4 Characterization of the MHEH performance

The performance of the hybrid multidirectional energy harvester is evaluated and the electromechanical couplings of the electromagnetic transducer, χ_{em} and κ_{em}, are important to be addressed. As discussed in Sect. 2, the value of these couplings is influenced by many con-

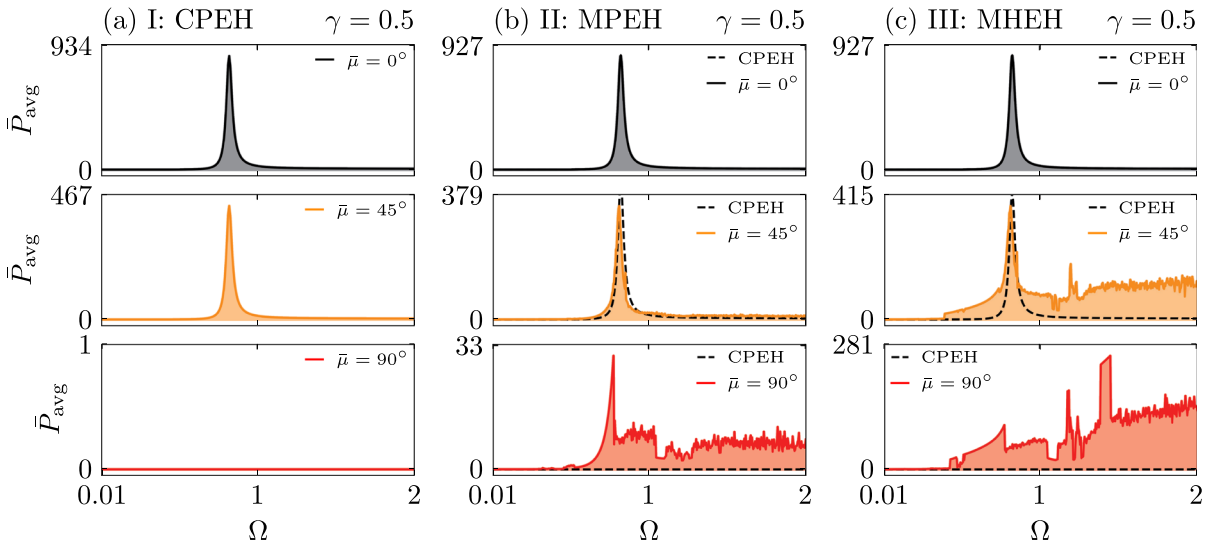

Fig. 9 $\bar{P}_{avg} \times \Omega$ diagrams for the Cases I, II, and III represented in Fig. 3 excited with different angles $\bar{\mu}$ for a normalized excitation amplitude of $\gamma = 0.5$. **a** Classical linear piezoelectric energy harvester (CPEH). **b** A comparison between the CPEH (dashed black lines) and the multidirectional piezoelectric energy harvester (MPEH). **c** A comparison between the CPEH (dashed black lines) and the proposed multidirectional hybrid energy harvester (MHEH). The values of $\bar{P}_{avg}$ are scaled by $\times 10^3$

struction characteristics of the transducer, especially the disposal of coils and internal magnet properties. In order to perform a general qualitative analysis of the MHEH, a variable is defined containing information of the electromagnetic transducer, based on the piezoelectric transducer. On this basis, consider the ratio between electromechanical couplings as

$$\eta = \frac{\chi_{em}}{\chi_{pz}} = \frac{\kappa_{em}}{\kappa_{pz}}. \tag{30}$$

Note that if $\eta = 1$, both transducers have the same coupling, while if $\eta < 1$, electromagnetic couplings have a lower value than the corresponding piezoelectric coupling. Alternatively, if $\eta > 1$, the electromagnetic couplings have a larger value than the corresponding piezoelectric couplings.

This section develops a characterization of the system performance by evaluating the influence of different parameters. The first subsection evaluates the influence of the electrical resistance parameters on the output power. On the other hand, the second subsection evaluates the effects of parameter η in the average output power of the MHEH. The analyses are carried out by considering three different configurations with different ratios of natural frequencies, Ω_s: 0.5, 1.0 and

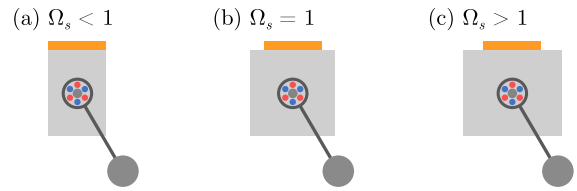

Fig. 10 Illustrative representation of the ratio of natural frequencies, Ω_s. **a** $\Omega_s < 1$, where the $\bar{x}$ direction is softer than the $\bar{z}$ direction (the beam's width is shorter than its height). **b** $\Omega_s = 1$, where both $\bar{x}$ and $\bar{z}$ directions have the same stiffness (both beam's width and height have the same length). **c** $\Omega_s > 1$, where the $\bar{x}$ direction is stiffer than the $\bar{z}$ direction (the beam's width is larger than its height)

1.5. An illustrative representation of the Ω_s parameter is presented in Fig. 10. The angle of excitation is maintained constant at $\bar{\mu} = 45°$ and the values of the remaining parameters are summarized in Table 1.

4.1 Influence of the electrical resistances, φ_{pz} and φ_{em}

The influence of the electrical resistance parameters is now of concern, establishing their effects on the average output power of the system. By considering a constant value of $\eta = 1$ and $\gamma = 0.1$, Average Output Power Diagrams (OPDs) are constructed to ana-

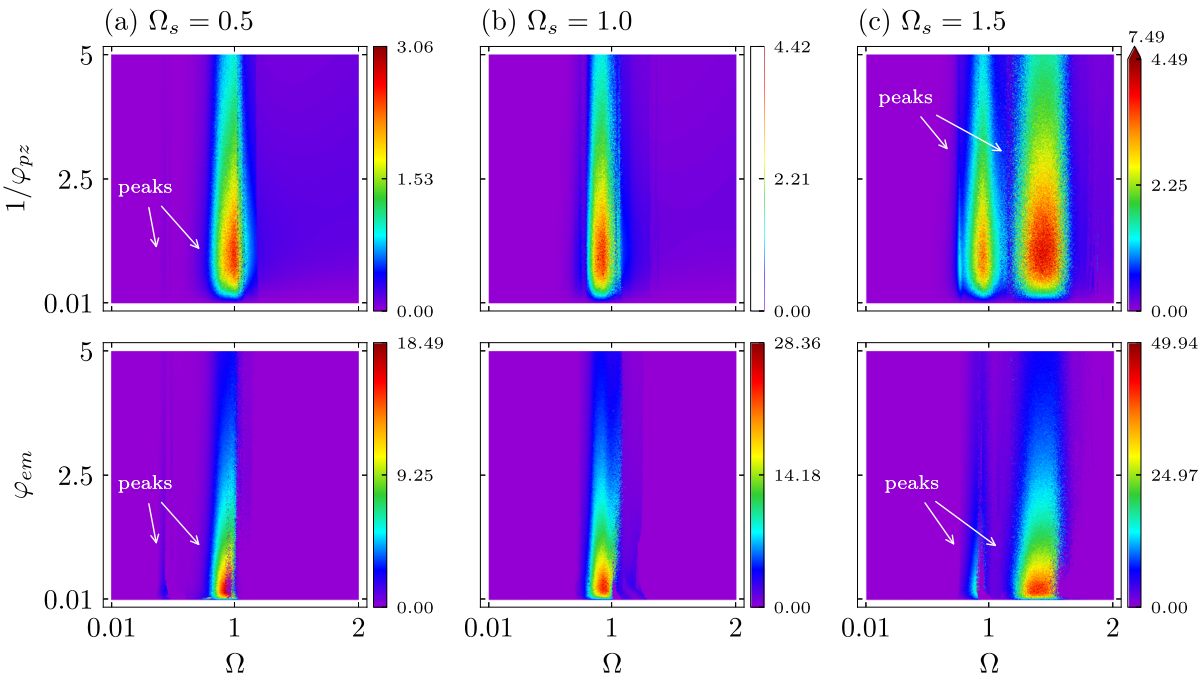

Fig. 11 OPDs for the normalized electrical resistance analysis, using a normalized excitation amplitude of $\gamma = 0.1$ and excitation angle of $\bar{\mu} = 45°$. Three groups with different ratios of natural frequencies of the main structure are defined: **a** with $\Omega_s = 0.5$, **b** $\Omega_s = 1.0$, and **c** $\Omega_s = 1.5$. Each group has two rows: The first row shows the output power for different values of conductance of the piezoelectric circuit ($1/\varphi_{pz}$), while the second row shows the output power for different values of the resistance of the electromagnetic circuit (φ_{em}). Rainbow colors in the colorbar indicate the level of average output power, $\bar{P}_{\text{avg}}$, achieved in each case. Colorbars that have an arrow at the top indicate that the range of colorbar values was limited for better display and the top value above the arrow is the maximum output power achieved. All values of $\bar{P}_{\text{avg}}$ are scaled by $\times 10^3$

lyze the influence of the normalized electrical resistance parameters, φ_{pz}, and φ_{em}, and the excitation frequency, Ω, in the output power of the system. These diagrams are built with a grid of 500 × 500 sample points, each of which is obtained from a time series integration. As in the previous diagrams, for each sample point, 800 excitation periods, T, are imposed at each integration, with the last 150 considered to be steady state. Then, the value of the average output power is computed based on the instantaneous output power values of the steady state part. Additionally, all sample points have the same initial conditions of $\bar{x}_0 = \dot{\bar{x}}_0 = \bar{z}_0 = \dot{\bar{z}}_0 = \bar{\phi}_0 = \dot{\bar{\phi}}_0 = \bar{v}_0 = \bar{I}_0 = 0$ to standardize the analysis.

Figure 11 shows these diagrams considering three configurations with different values of Ω_s. Each column of Fig. 11 is related to one different configuration: Fig. 11a for $\Omega_s = 0.5$, that is, the $\bar{z}$ direction is stiffer than the $\bar{x}$ direction; Fig. 11b for $\Omega_s = 1.0$, where both stiffness of each direction are equal; and Fig. 11c for $\Omega = 1.5$, showing a configuration with a stiffer $\bar{x}$ direction than the $\bar{z}$ direction. The first row of each configuration shows the OPD for the values of the normalized conductance of the piezoelectric circuit, $1/\varphi_{pz}$. For all configurations, the optimal value of the normalized conductance is shown to be around $1/\varphi_{pz} = 1$. Additionally, the second row of each configuration shows the OPD for the values of the normalized resistance of the electromagnetic circuit, φ_{em}. As in the previous case, the three configurations show similar regions of optimal resistance around $\varphi_{em} = 0.25$.

In this case, it should be pointed out that the increase of Ω_s produces an increase in the maximum output power in both piezoelectric and electromagnetic transducer circuits. Additionally, the presence of two peaks of output power in the first and third cases, as pointed out by the white arrows, occurs due to the shift of the resonance regions caused by the change of Ω_s.

4.2 Influence of the ratio between electromechanical couplings, η

The ratio between electromechanical couplings, η, is now of concern addressing the evaluation of its effects on the average output powers of the MHEH. Three values of η are selected: 0.2, 0.5 and 0.8. For each value of η, the same three configurations with different Ω_s values are evaluated, as discussed in the previous subsection. Results are summarized in $\bar{P}_{\text{avg}} \times \Omega$ diagrams displayed in Figs. 12, 13, and 14, which are divided into three sections based on different values of normalized excitation amplitude of $\gamma = 0.1$, $\gamma = 0.25$, and $\gamma = 0.5$. In these Figures, dashed lines represent the $\bar{P}_{\text{avg}}$ for the CPEH, serving as a reference for comparison. Additionally, these diagrams include red curves that represent the average output power associated with the piezoelectric element, $\bar{P}_{pz}$, orange curves that represent the average output power of the electromagnetic transducer, $\bar{P}_{em}$, and purple curves that represent the total average output power of the MHEH, $\bar{P}_{\text{avg}}$. Note that all values of power are scaled by $\times 10^3$ for better representation.

Figure 12 represents the case with $\eta = 0.2$. Figure 12a illustrates that, given this particular value of η and low excitation amplitudes ($\gamma = 0.1$), the MHEH does not enhance energy conversion to a degree that justifies its use over the CPEH. This observation holds true for $\gamma = 0.25$ and $\gamma = 0.5$, as displayed in Figs. 12b and 12c. However, under these conditions, the piezoelectric output power, denoted as $\bar{P}_{pz}$, exhibits a significant increase.

Additionally, Fig. 13 shows the results for a scenario with $\eta = 0.5$. For low excitation amplitude values ($\gamma = 0.1$), the CPEH is still advantageous for $\Omega_s = 0.5$. Alternatively, for the cases with $\Omega_s = 1.0$ and $\Omega_s = 1.5$, the performances became comparable or even better than the CPEH. For medium values of excitation amplitude ($\gamma = 0.25$), as displayed in Fig. 13b, this value of η is suitable for replacing the CPEH as both piezoelectric and electromagnetic transducers contribute effectively for the energy conversion.

For greater values of excitation amplitude ($\gamma = 0.5$), as displayed in Fig. 13c, only the piezoelectric transducer contributes effectively to the energy conversion.

Furthermore, Fig. 14 illustrates the case where the value of η is increased to 0.8. In this case, nearly all combinations of Ω_s and γ demonstrate the benefits of employing the MHEH. This is because, in every scenario, the output powers are comparable to or exceed those presented by the CPEH. Consequently, it follows that the optimal ratio of electromechanical couplings is around $\eta = 0.8$, given this set of parameters, where both piezoelectric and electromagnetic transducers contribute effectively to the energy conversion. For higher values of η, the electromagnetic transducer should convert much more than the piezoelectric element.

Finally, by observing the values of output power presented in Figs. 12, 13, and 14, as well as in Fig. 11 of the previous section, it is revealed that the increase of Ω_s tends to increase the bandwidth. This behavior can be attributed to a rightward shift in the resonance region associated with the x direction, prompted by the change in Ω_s. Notably, the high-performance region, characterized by high-amplitude structural motion, initiates near the resonance region of the z direction, with the dynamical attractor persisting as Ω increases. Specifically, the system initial conditions at each frequency step correspond to the final conditions of the preceding step. When excited near the resonance region of the x direction, the motion in the z direction diminishes, while motion in the x direction intensifies, resulting in increased angular motion of the pendulum associated with large amplitude oscillations and rotations. Conversely, when the system is excited far from resonance regions, performance abruptly drops. This behavior occurs at higher frequencies. Moreover, as excitation amplitude increases, this decline in performance occurs at even higher frequencies, reflecting the increased input energy required to maintain the system within a high-amplitude attractor.

5 Conclusions

This work presents a novel hybrid multidirectional energy harvester that can enhance the performance of cantilever-based harvesters when subjected to multidirectional excitations. The proposed system employs a pendulum structure to achieve multidirectionality and multiple transduction mechanisms to enhance energy conversion. Specifically, a piezoelectric transducer is attached to the cantilever structure, and an electromagnetic transducer is incorporated into the rotational support of the pendulum. Three distinct harvesters of the same class are compared: (1) the classical piezoelectric energy harvester (CPEH), which converts

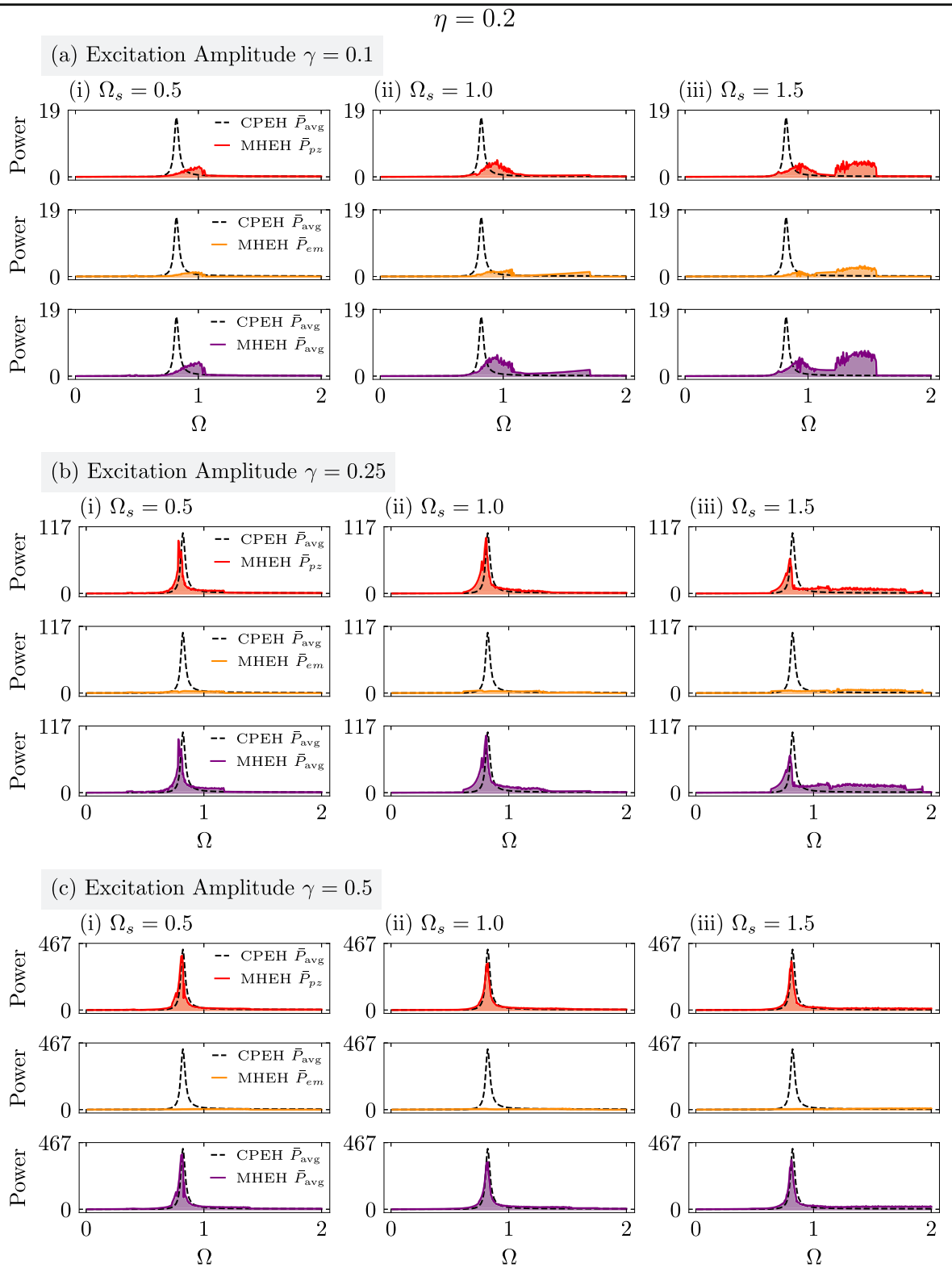

Fig. 12 $\Omega \times \bar{P}_{\text{avg}}$ diagrams for $\eta = 0.2$. Three excitation amplitude values are chosen: **a** $\gamma = 0.1$, **b** $\gamma = 0.25$, and **c** $\gamma = 0.5$. For each value of γ, three configurations are selected with (i) $\Omega_s = 0.5$, (ii) $\Omega_s = 1$ and (iii) $\Omega_s = 1.5$. In each plot, dashed lines represent the $\bar{P}_{\text{avg}}$ for the CPEH, serving as a reference for comparison. Additionally, red curves represent $\bar{P}_{pz}$, orange curves represent $\bar{P}_{em}$, and purple curves represent $\bar{P}_{\text{avg}}$, all for the MHEH. All values of power are scaled by $\times 10^3$

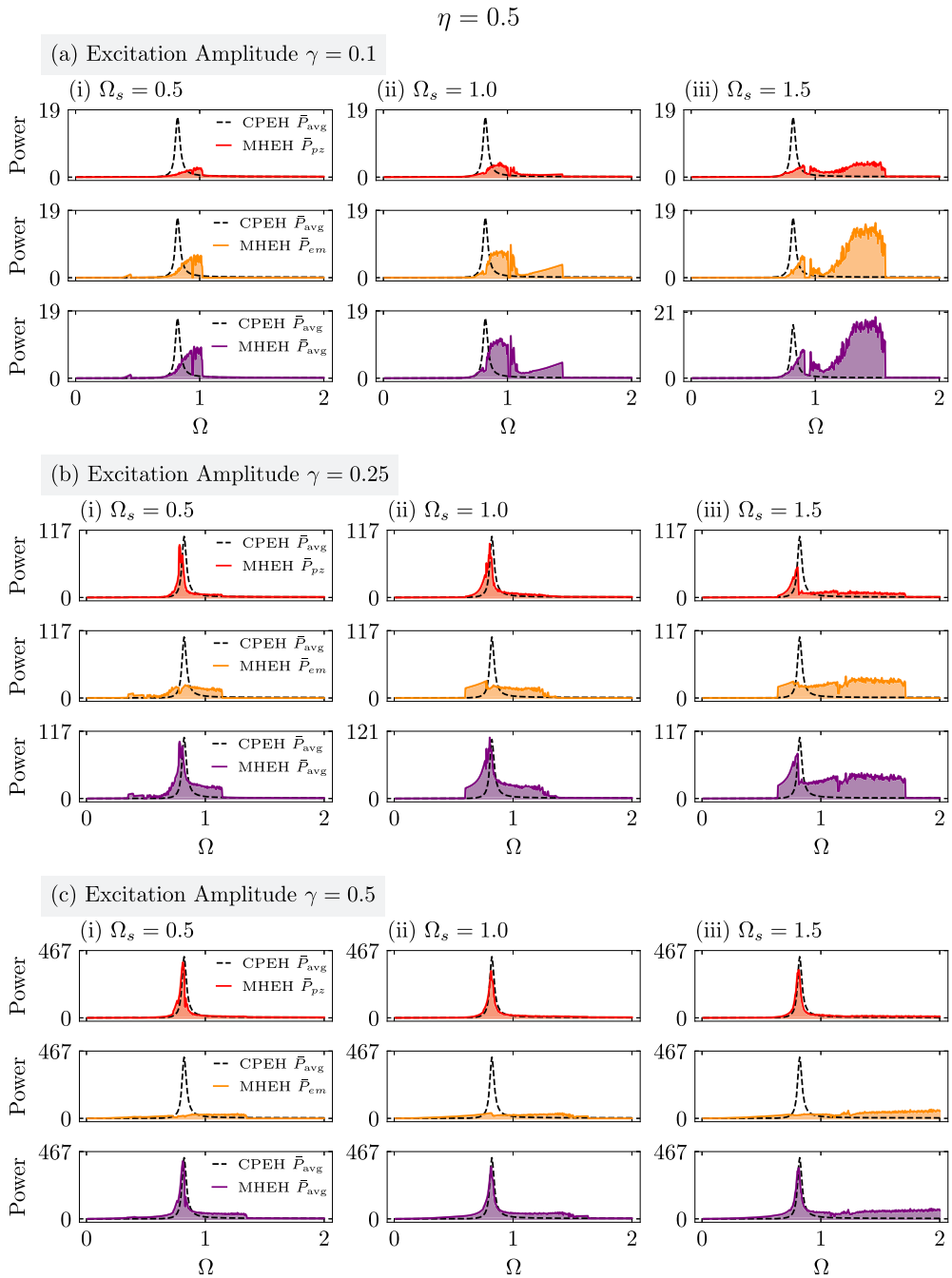

Fig. 13 $\Omega \times \bar{P}_{\text{avg}}$ diagrams for $\eta = 0.5$. Three excitation amplitude values are chosen: **a** $\gamma = 0.1$, (b) $\gamma = 0.25$, and (c) $\gamma = 0.5$. For each value of γ, three configurations are selected with (i) $\Omega_s = 0.5$, (ii) $\Omega_s = 1$ and (iii) $\Omega_s = 1.5$. In each plot, dashed lines represent the $\bar{P}_{\text{avg}}$ for the CPEH, serving as a reference for comparison. Additionally, red curves represent $\bar{P}_{pz}$, orange curves represent $\bar{P}_{em}$, and purple curves represent $\bar{P}_{\text{avg}}$, all for the MHEH. All values of power are scaled by $\times 10^3$

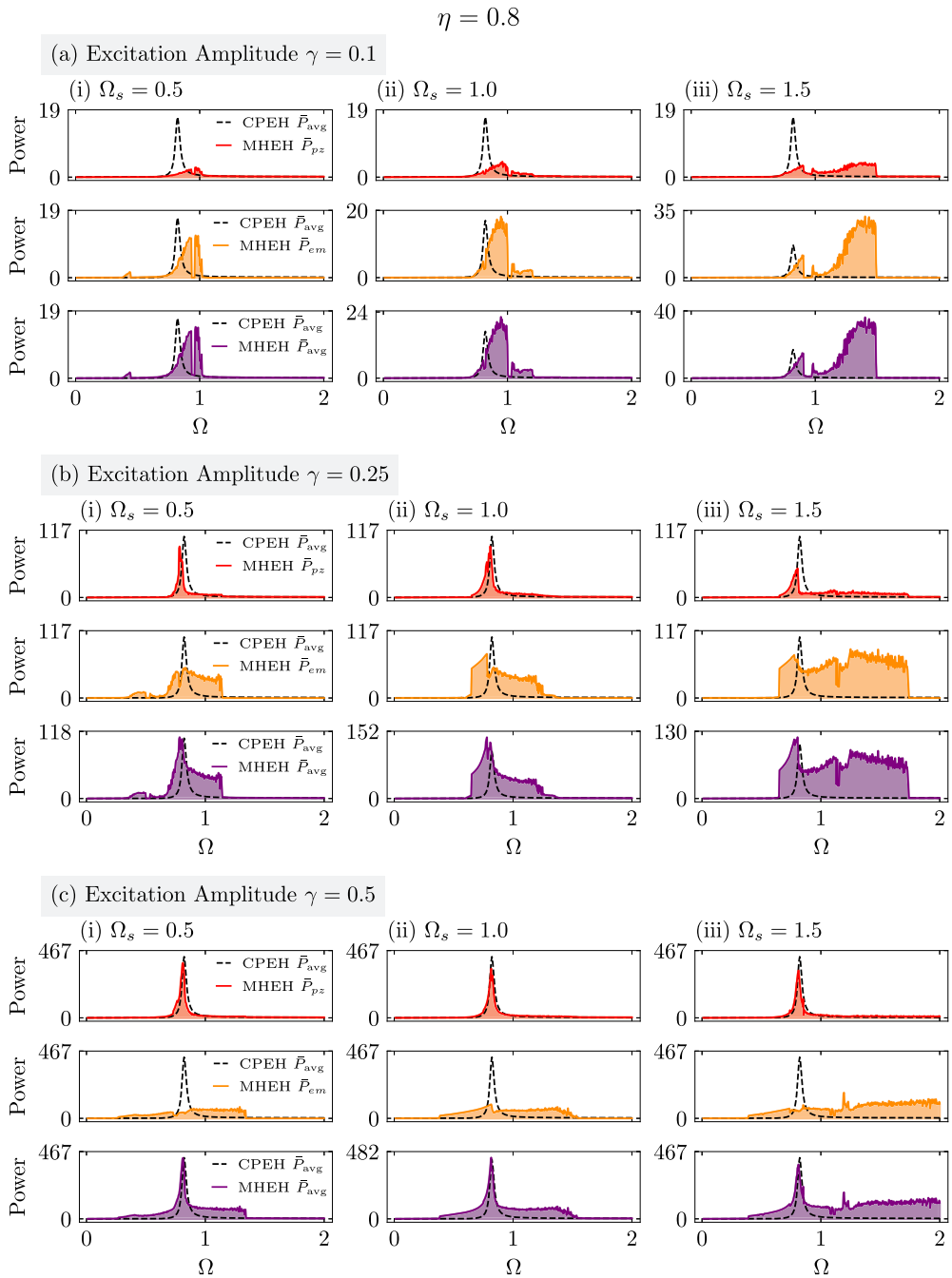

Fig. 14 $\Omega \times \bar{P}_{\text{avg}}$ diagrams for $\eta = 0.5$. Three excitation amplitude values are chosen: **a** $\gamma = 0.1$, **b** $\gamma = 0.25$, and **c** $\gamma = 0.5$. For each value of γ, three configurations are selected with (i) $\Omega_s = 0.5$, (ii) $\Omega_s = 1$ and (iii) $\Omega_s = 1.5$. In each plot, dashed lines represent the $\bar{P}_{\text{avg}}$ for the CPEH, serving as a reference for comparison. Additionally, red curves represent $\bar{P}_{pz}$, orange curves represent $\bar{P}_{em}$, and purple curves represent $\bar{P}_{\text{avg}}$, all for the MHEH. All values of power are scaled by $\times 10^3$

energy in a single direction; (2) the multidirectional energy harvester (MPEH), comprising the same structure as the CPEH combined with a pendulum; and (3) the proposed multidirectional hybrid energy harvester (MHEH), being an evolution of the previous harvester.

A theoretical model is established to describe the main characteristics of the three harvesters and numerical simulations are carried out in order to compare their performances. Results demonstrate that the use of the pendulum structure to achieve efficient multidirectional conversion (utilizing the MPEH), is insufficient since it can work as a dynamical absorber, thereby reducing the system overall performance when compared to its classic counterpart (CPEH). Alternatively, by employing the proposed MHEH, results show an impressive increase of performance in both maximum output power and bandwidth when compared to the CPEH, demonstrating that the proposed system not only retains the desirable characteristics of the MPEH but can also effectively address its limitations.

The performance of the MHEH system is analyzed by examining the influence of key parameters. Initially, the optimal resistance parameters are identified in order to find the maximum output power regions of both transducers. Using the optimal resistance values, it is demonstrated that the ratio of electromechanical couplings ($\eta = \chi_{em}/\chi_{pz} = \kappa_{em}/\kappa_{pz}$) should be approximately 0.8 for both piezoelectric and electromagnetic transducers to effectively contribute to energy conversion. If this ratio is too low, the piezoelectric element dominates the energy conversion, whereas if η is too high, the electromagnetic transducer converts more energy than the piezoelectric element. Furthermore, it is observed that the electromagnetic transducer predominantly handles the energy conversion at low excitation amplitudes. Alternatively, the piezoelectric transducer takes precedence in energy conversion as the excitation amplitudes increase. The influence of the natural frequencies of the structure (natural frequencies in each direction of the Cartesian plane) are evaluated and results show that a stiffer horizontal direction (perpendicular to the direction of gravity) enhances the bandwidth of the system.

Overall, this study establishes the hybrid multidirectional energy harvester as a solution that maintains the desirable multidirectional characteristics while mitigating the drawbacks associated with attaching a pendulum without an associated transducer.

Funding The authors would like to acknowledge the support of the Brazilian Research Agencies CNPq (Conselho Nacional de Desenvolvimento Científico e Tecnológico), CAPES (Coordenação de Aperfeiçoamento de Pessoal de Nível Superior) and FAPERJ (Fundação Carlos Chagas Filho de Amparo à Pesquisa do Estado do Rio de Janeiro) and through the INCT-EIE (National Institute of Science and Technology - Smart Structures in Engineering), CNPq, CAPES and FAPEMIG (Fundação de Amparo à Pesquisa do Estado de Minas Gerais). The support of the AFOSR (Air Force Office of Scientific Research) is also acknowledged. Moreover, the authors also appreciate the use of the computational resources of the NACAD (Advanced High-Performance Computing Nucleus).

Data availibility The datasets generated during and/or analyzed during the current study are available from the corresponding author upon reasonable request.

Declarations

Conflict of interest The authors declare that they have no Conflict of interest.

References

1. Abdelkareem, M.A., Jing, X., Eldaly, A.B., Choy, Y.: 3-dof x-structured piezoelectric harvesters for multidirectional low-frequency vibration energy harvesting. Mech. Syst. Signal Process. **200**, 110616 (2023). https://doi.org/10.1016/j.ymssp.2023.110616
2. Adeodato, A., Duarte, B.T., Monteiro, L.L.S., Pacheco, P.M.C., Savi, M.A.: Synergistic use of piezoelectric and shape memory alloy elements for vibration-based energy harvesting. Int. J. Mech. Sci. **194**, 106206 (2021). https://doi.org/10.1016/j.ijmecsci.2020.106206
3. Ai, R., Monteiro, L.L.S., Monteiro, P.C.C., Pacheco, P.M.C.L., Savi, M.A.: Piezoelectric vibration-based energy harvesting enhancement exploiting nonsmoothness. Actuators (2019). https://doi.org/10.3390/act8010025
4. Caetano, V.J., Savi, M.A.: Multimodal pizza-shaped piezoelectric vibration-based energy harvesters. J. Intell. Mater. Syst. Struct. **32**(20), 2505–2528 (2021). https://doi.org/10.1177/1045389X211006910
5. Caetano, V.J., Savi, M.A.: Star-shaped piezoelectric mechanical energy harvesters for multidirectional sources. Int. J. Mech. Sci. **215**, 106962 (2022). https://doi.org/10.1016/j.ijmecsci.2021.106962
6. Cepnik, C., Lausecker, R., Wallrabe, U.: Review on electrodynamic energy harvesters-a classification approach. Micromachines **4**(2), 168–196 (2013). https://doi.org/10.3390/mi4020168
7. Chen, J., Bao, B., Liu, J., Wu, Y., Wang, Q.: Pendulum energy harvesters: a review. Energies (2022). https://doi.org/10.3390/en15228674
8. Chung, J., Song, M., Chung, S.-H., Choi, W., Lee, S., Lin, Z.-H., Hong, J., Lee, S.: Triangulated cylinder origami-based

piezoelectric/triboelectric hybrid generator to harvest coupled axial and rotational motion. Research (2021). https://doi.org/10.34133/2021/7248579
9. Clementi, G., Cottone, F., Di Michele, A., Gammaitoni, L., Mattarelli, M., Perna, G., López-Suárez, M., Baglio, S., Trigona, C., Neri, I.: Review on innovative piezoelectric materials for mechanical energy harvesting. Energies (2022). https://doi.org/10.3390/en15176227
10. Costa, L.G., da Silva Monteiro, L.L., Pacheco, P.M.C.L., Savi, M.A.: A parametric analysis of the nonlinear dynamics of bistable vibration-based piezoelectric energy harvesters. J. Intell. Mater. Syst. Struct. **32**(7), 699–723 (2021). https://doi.org/10.1177/1045389X20963188
11. Costa, L.G., Monteiro, L.L.S., Savi, M.A.: Multistability investigation for improved performance in a compact nonlinear energy harvester. J. Braz. Soc. Mech. Sci. Eng. **46**(4), 212 (2024). https://doi.org/10.1007/s40430-024-04766-5
12. Costa, L.G., Savi, M.A.: Nonlinear dynamics of a compact and multistable mechanical energy harvester. Int. J. Mech. Sci. **262**, 108731 (2024). https://doi.org/10.1016/j.ijmecsci.2023.108731
13. Dagdeviren, C., Yang, B.D., Su, Y., Tran, P.L., Joe, P., Anderson, E., Xia, J., Doraiswamy, V., Dehdashti, B., Feng, X., Lu, B., Poston, R., Khalpey, Z., Ghaffari, R., Huang, Y., Slepian, M.J., Rogers, J.A.: Conformal piezoelectric energy harvesting and storage from motions of the heart, lung, and diaphragm. Proc. Natl. Acad. Sci. **111**(5), 1927–1932 (2014). https://doi.org/10.1073/pnas.1317233111
14. De Paula, A.S., Inman, D.J., Savi, M.A.: Energy harvesting in a nonlinear piezomagnetoelastic beam subjected to random excitation. Mech. Syst. Signal Process. **54–55**, 405–416 (2015). https://doi.org/10.1016/j.ymssp.2014.08.020
15. Delnavaz, A., Voix, J.: Flexible piezoelectric energy harvesting from jaw movements. Smart Mater. Struct. **23**(10), 105020 (2014). https://doi.org/10.1088/0964-1726/23/10/105020
16. Demartino, C., Quaranta, G., Maruccio, C., Pakrashi, V.: Feasibility of energy harvesting from vertical pedestrian-induced vibrations of footbridges for smart monitoring applications. Comput.-Aid. Civil Infrastruct. Eng. **37**(8), 1044–1065 (2022). https://doi.org/10.1111/mice.12777
17. Deterre, M., Lefeuvre, E., Dufour-Gergam, E.: An active piezoelectric energy extraction method for pressure energy harvesting. Smart Mater. Struct. **21**(8), 085004 (2012). https://doi.org/10.1088/0964-1726/21/8/085004
18. Dutoit, N.E., Wardle, B.L., Kim, S.-G.: Design considerations for mems-scale piezoelectric mechanical vibration energy harvesters. Integr. Ferroelectr. **71**(1), 121–160 (2005). https://doi.org/10.1080/10584580590964574
19. Egbe, K.-J.I., Matin Nazar, A., Jiao, P.: Piezoelectric-triboelectric-electromagnetic hybrid rotational energy harvesters (h-reh). Int. J. Mech. Sci. **235**, 107722 (2022). https://doi.org/10.1016/j.ijmecsci.2022.107722
20. Elhalwagy, A.M., Ghoneem, M.Y.M., Elhadidi, M.: Feasibility study for using piezoelectric energy harvesting floor in buildings' interior spaces. Energy Procedia, **115**, 114–126 (2017). International Conference - Alternative and Renewable Energy Quest, AREQ 2017, 1-3 February 2017, Spain. https://doi.org/10.1016/j.egypro.2017.05.012
21. Erturk, A.: Piezoelectric energy harvesting for civil infrastructure system applications: moving loads and surface strain fluctuations. J. Intell. Mater. Syst. Struct. **22**(17), 1959–1973 (2011). https://doi.org/10.1177/1045389X11420593
22. Fu, H., Jiang, J., Hu, S., Rao, J., Theodossiades, S.: A multi-stable ultra-low frequency energy harvester using a nonlinear pendulum and piezoelectric transduction for self-powered sensing. Mech. Syst. Signal Process. **189**, 110034 (2023). https://doi.org/10.1016/j.ymssp.2022.110034
23. Fu, H., Mei, X., Yurchenko, D., Zhou, S., Theodossiades, S., Nakano, K., Yeatman, E.M.: Rotational energy harvesting for self-powered sensing. Joule **5**(5), 1074–1118 (2021). https://doi.org/10.1016/j.joule.2021.03.006
24. Gao, L., Lu, S., Xie, W., Chen, X., Wu, L., Wang, T., Wang, A., Yue, C., Tong, D., Lei, W., Yu, H., He, X., Mu, X., Wang, Z.L., Yang, Y.: A self-powered and self-functional tracking system based on triboelectric-electromagnetic hybridized blue energy harvesting module. Nano Energy **72**, 104684 (2020). https://doi.org/10.1016/j.nanoen.2020.104684
25. Halim, M.A., Kabir, M.H., Cho, H., Park, J.Y.: A frequency up-converted hybrid energy harvester using transverse impact-driven piezoelectric bimorph for human-limb motion. Micromachines (2019). https://doi.org/10.3390/mi10100701
26. Haroun, A., Tarek, M., Mosleh, M., Ismail, F.: Recent progress on triboelectric nanogenerators for vibration energy harvesting and vibration sensing. Nanomaterials (2022). https://doi.org/10.3390/nano12172960
27. IEA. Renewables 2021 - analysis and forecast to 2026. Technical report, International Energy Agency - IEA, Paris (2021)
28. Izadgoshasb, I.: Piezoelectric energy harvesting towards self-powered internet of things (iot) sensors in smart cities. Sensors (2021). https://doi.org/10.3390/s21248332
29. Jiang, X., Liu, Y., Wei, J., Yang, H., Yin, B., Qin, H., Wang, W.: Multidirectional piezoelectric vibration energy harvester based on cam rotor mechanism. Micromachines (2023). https://doi.org/10.3390/mi14061159
30. Lee, J., Choi, B.: Development of a piezoelectric energy harvesting system for implementing wireless sensors on the tires. Energy Convers. Manag. **78**, 32–38 (2014). https://doi.org/10.1016/j.enconman.2013.09.054
31. Li, H., Lu, J., Myjak, M.J., Liss, S.A., Brown, R.S., Tian, C., Deng, Z.D.: An implantable biomechanical energy harvester for animal monitoring devices. Nano Energy **98**, 107290 (2022). https://doi.org/10.1016/j.nanoen.2022.107290
32. Liu, H., Hou, C., Lin, J., Li, Y., Shi, Q., Chen, T., Sun, L., Lee, C.: A non-resonant rotational electromagnetic energy harvester for low-frequency and irregular human motion. Appl. Phys. Lett. **113**(20), 203901 (2018). https://doi.org/10.1063/1.5053945
33. Liu, Y., Khanbareh, H., Halim, M.A., Feeney, A., Zhang, X., Heidari, H., Ghannam, R.: Piezoelectric energy harvesting for self-powered wearable upper limb applications. Nano Select **2**(8), 1459–1479 (2021). https://doi.org/10.1002/nano.202000242
34. Lu, K., Hu, R., Wang, X., Deng, Z.: Multi-directional and ultra-low frequency energy harvester utilizing tunable buckled piezoelectric film. Mech. Syst. Signal Process. **210**, 111137 (2024). https://doi.org/10.1016/j.ymssp.2024.111137

35. Meirovitch, L.: Methods of Analytical Dynamics. Dover Publications, Advanced engineering series (2010)
36. Nabavi, S.F., Farshidianfar, A., Afsharfard, A.: Novel piezoelectric-based ocean wave energy harvesting from offshore buoys. Appl. Ocean Res. **76**, 174–183 (2018). https://doi.org/10.1016/j.apor.2018.05.005
37. Pan, J., Qin, W., Deng, W., Zhang, P., Zhou, Z.: Harvesting weak vibration energy by integrating piezoelectric inverted beam and pendulum. Energy **227**, 120374 (2021). https://doi.org/10.1016/j.energy.2021.120374
38. Pan, J.-N., Qin, W.-Y., Deng, W.-Z., Zhou, H.-L.: Harvesting base vibration energy by a piezoelectric inverted beam with pendulum*. Chin. Phys. B **28**(1), 017701 (2019). https://doi.org/10.1088/1674-1056/28/1/017701
39. Peigney, M., Siegert, D.: Piezoelectric energy harvesting from traffic-induced bridge vibrations. Smart Mater. Struct. **22**(9), 095019 (2013). https://doi.org/10.1088/0964-1726/22/9/095019
40. Preumont, A.: Mechatronics: Dynamics of Electromechanical and Piezoelectric Systems. Springer, Dordrecht (2006). https://doi.org/10.1007/1-4020-4696-0
41. Sebald, G., Tung, N.T., Taxil, G., Ducharne, B., Chavez, J., Ono, T., Kuwano, H., Lefeuvre, E., Lallart, M.: Piezoelectric small scale generator: towards near-joule output energy generation. Smart Mater. Struct. **32**(8), 085009 (2023). https://doi.org/10.1088/1361-665X/acdf31
42. Stanton, S.C., McGehee, C.C., Mann, B.P.: Reversible hysteresis for broadband magnetopiezoelastic energy harvesting. Appl. Phys. Lett. **95**(17), 174103 (2009). https://doi.org/10.1063/1.3253710
43. Steffen, W., Rockström, J., Richardson, K., Lenton, T.M., Folke, C., Liverman, D., Summerhayes, C.P., Barnosky, A.D., Cornell, S.E., Crucifix, M., Donges, J.F., Fetzer, I., Lade, S.J., Scheffer, M., Winkelmann, R., Schellnhuber, H.J.: Trajectories of the earth system in the anthropocene. Proc. Natl. Acad. Sci. **115**(33), 8252–8259 (2018). https://doi.org/10.1073/pnas.1810141115
44. Tavares, R., Ruderman, M.: Energy harvesting using piezoelectric transducers for suspension systems. Mechatronics **65**, 102294 (2020). https://doi.org/10.1016/j.mechatronics.2019.102294
45. Toprak, A., Tigli, O.: Piezoelectric energy harvesting: State-of-the-art and challenges. Appl. Phys. Rev. **1**(3), 031104 (2014). https://doi.org/10.1063/1.4896166
46. Wang, C., Zhao, J., Li, Q., Li, Y.: Optimization design and experimental investigation of piezoelectric energy harvesting devices for pavement. Appl. Energy **229**, 18–30 (2018). https://doi.org/10.1016/j.apenergy.2018.07.036
47. Wang, T.: Pendulum-based vibration energy harvesting: mechanisms, transducer integration, and applications. Energy Convers. Manag. **276**, 116469 (2023). https://doi.org/10.1016/j.enconman.2022.116469
48. Wu, Y., Li, S., Fan, K., Ji, H., Qiu, J.: Investigation of an ultra-low frequency piezoelectric energy harvester with high frequency up-conversion factor caused by internal resonance mechanism. Mech. Syst. Signal Process. **162**, 108038 (2022). https://doi.org/10.1016/j.ymssp.2021.108038
49. Wu, Y., Qiu, J., Zhou, S., Ji, H., Chen, Y., Li, S.: A piezoelectric spring pendulum oscillator used for multi-directional and ultra-low frequency vibration energy harvesting. Appl. Energy **231**, 600–614 (2018). https://doi.org/10.1016/j.apenergy.2018.09.082
50. Xiao, Y., Niu, M., Yang, L., Liu, J., Lv, X., Yang, P.: Integrated triboelectric-electromagnetic-piezoelectric self-rebounding energy harvester for human energy harvesting. Adv. Mater. Technol. **7**(11), 2200340 (2022). https://doi.org/10.1002/admt.202200340
51. Xu, J., Tang, J.: Multi-directional energy harvesting by piezoelectric cantilever-pendulum with internal resonance. Appl. Phys. Lett. (2015). https://doi.org/10.1063/1.4936607
52. Yang, T., Cao, Q.: Dynamics and performance evaluation of a novel tristable hybrid energy harvester for ultra-low level vibration resources. Int. J. Mech. Sci. **156**, 123–136 (2019). https://doi.org/10.1016/j.ijmecsci.2019.03.034
53. Yuan, J.H., Yang, Y.Z., Zhang, Y.H.: A piezoelectric energy harvester with light-activated shape memory polymers. Ferroelectrics **550**(1), 98–111 (2019). https://doi.org/10.1080/00150193.2019.1652500
54. Zhao, L.-C., Zou, H.-X., Gao, Q.-H., Yan, G., Liu, F.-R., Tan, T., Wei, K.-X., Zhang, W.-M.: Magnetically modulated orbit for human motion energy harvesting. Appl. Phys. Lett. **115**(26), 263902 (2019). https://doi.org/10.1063/1.5131193
55. Zhong, X., Yang, Y., Wang, X., Wang, Z.L.: Rotating-disk-based hybridized electromagnetic-triboelectric nanogenerator for scavenging biomechanical energy as a mobile power source. Nano Energy **13**, 771–780 (2015). https://doi.org/10.1016/j.nanoen.2015.03.012
56. Zhu, J., Liu, X., Shi, Q., He, T., Sun, Z., Guo, X., Liu, W., Sulaiman, O.B., Dong, B., Lee, C.: Development trends and perspectives of future sensors and mems/nems. Micromachines (2020). https://doi.org/10.3390/mi11010007
57. Zuo, L., Tang, X.: Large-scale vibration energy harvesting. J. Intell. Mater. Syst. Struct. **24**(11), 1405–1430 (2013). https://doi.org/10.1177/1045389X13486707